Design and Performance of Hybrid Arrays of Mo/Au Bilayer Transition-Edge Sensors

Wonsik Yoon, Joseph S. Adams, Simon R. Bandler, Gabriele L. Betancourt-Martinez, Meng P. Chiao, Meng-Ping Chang, James A. Chervenak, Aaron Datesman, Megan E. Eckart, Audrey J. Ewin, Fred Michael Finkbeiner, Jong Yoon Ha, Richard Kelley, Caroline A. Kilbourne, Antoine R. Miniussi, Frederick Scott Porter, John E. Sadleir, Kazuhiro Sakai, Stephen James Smith, Nicholas A. Wakeham, and Edward Wassell

***Abstract*—For future X-ray astrophysics missions, X-ray microcalorimeters can be optimized with different properties in different regions of the focal plane. This approach has the potential to improve microcalorimeter instrument capabilities with efficient use of instrument resources. For example a point-source array optimized for high angular resolution, high count-rate observations could be accompanied by a main array to expand the field of view for diffuse observations. In this approach, it is desirable to be able to simultaneously optimize different transition-edge sensor (TES) geometries on a single wafer design. The key properties of TESs such as transition temperature and shape are a strong function of size and geometry due to the complex interplay between the proximity effect from the superconducting bias electrodes and the normal metal features used for noise suppression and absorber contact. As a result, devices fabricated with the same deposited layer but with different sizes will have different transition temperatures and different response to X-ray events. In this paper, we present measurements of the transition temperature and properties of devices with different sizes and normal metal features, and discuss how by tuning the geometry we can achieve the desired pixel parameters for a given application. We also describe measurements of transition properties from large-format hybrid arrays containing three different pixel types.**

***Index Terms*—Transition-edge sensors, hybrid array, transition temperature.**

I. Introduction

FUTURE X-ray astrophysics missions require large field of view, high spatial resolution, high energy resolution, high quantum efficiency and high count rate. Superconducting transition-edge sensors (TES) are one of the microcalorimeter technologies with the potential to meet such requirements [1], [2]. TESs have been baselined for the detector array of the X-ray Integral Field Unit (X-IFU) instrument on the Advanced Telescope for High-Energy Astrophysics (Athena) mission selected by ESA [3]. The X-IFU requires ~4000 pixels. The simplest approach is to build a large uniform array in which all pixels can meet all requirements.

We have been developing uniform arrays of pixels on a 0.25 mm pitch with the potential to meet the X-IFU energy resolution requirements of $\Delta E_{\mathrm{FWHM}} < 2.5$ eV, with count rates commensurate with the ability to observe X-ray point sources with the intensity of 1 mCrab. For the area of X-ray optic envisioned, with 5" angular resolution and a 12 meter focal length, this corresponds to a total point source count rate of ~90 counts per second (cps) with 80% throughput, which in turn corresponds to a maximum per pixel count rate of ~50 cps since the X-rays will always be spread out a few pixels [4].

This instrument also has a count rate goal that significantly exceeds the requirements. The goal is to accommodate count rates which are ten times higher, still at 80% throughput and the required energy resolution, which would be extremely challenging with 0.25 mm pixels. One of the ways to make this count-rate goal achievable is to use smaller pixels to over-sample the 5" point spread function of the X-ray mirror. By spreading the counts over many more pixels, and indeed by optimizing these smaller pixels for high count rate, the mission goals become achievable. A uniform array of much smaller pixels would

Manuscript received September 6, 2016; accepted January 14, 2017. Date of publication January 19, 2017; date of current version February 10, 2017.

W. Yoon and N. A. Wakeham are with the NASA Goddard Space Flight Center, Greenbelt, MD 20771 USA, and also with the NASA Postdoctoral Program—Universities Space Research Association, Columbia, MD 21046 USA (e-mail: wonsik.yoon@nasa.gov; Nicholas.a.wakeham@nasa.gov).

J. S. Adams, M. P. Chiao, and S. J. Smith are with the NASA Goddard Space Flight Center, Greenbelt, MD 20771 USA, and also with the University of Maryland, Baltimore County, Baltimore, MD 21250 USA (e-mail: Joseph.S.Adams@nasa.gov; meng.p.chiao@nasa.gov; stephen.j.smith@nasa.gov).

S. R. Bandler, J. A. Chervenak, M. E. Eckart, A. J. Ewin, R. Kelley, C. A. Kilbourne, F. S. Porter, and J. E. Sadleir are with the NASA Goddard Space Flight Center, Greenbelt, MD 20771 USA (e-mail: Simon.R.Bandler@nasa.gov; James.A.Chervenak@nasa.gov; Megan.E.Eckart@nasa.gov; Audrey.J.Ewin@nasa.gov; Richard.L.Kelley@nasa.gov; Caroline.A.Kilbourne@nasa.gov; Frederick.S.Porter@nasa.gov; john.e.sadleir@nasa.gov).

G. L. Betancourt-Martinez is with the NASA Goddard Space Flight Center, Greenbelt, MD 20771 USA, and also with the University of Maryland, College Park, MD 20742 USA (e-mail: Gabriele.L.Betancourt-Martinez@nasa.gov).

A. Datesman, M. Chang, and E. Wassell are with the NASA Goddard Space Flight Center, Greenbelt, MD 20771 USA, and also with the SGT, Inc., Greenbelt, MD 20706 USA (e-mail: aaron.m.datesman@nasa.gov; meng-ping.chang@nasa.gov; edward.wassell@nasa.gov).

J. Ha is with the NASA Goddard Space Flight Center, Greenbelt, MD 20771 USA, and also with the SB Microsystems, Inc., Glen Burnie, MD 21061 USA (e-mail: jongyoon.ha@sbmicrosystems.us).

F. M. Finkbeiner is with the NASA Goddard Space Flight Center, Greenbelt, MD 20771 USA, and also with the Wyle Information Systems, McLean, VA 22102 USA (e-mail: Fred.M.Finkbeiner@nasa.gov).

K. Sakai and A. R. Miniussi are with the NASA Goddard Space Flight Center, Greenbelt, MD 20771 USA, and also with the Universities Space Research Association, Columbia, MD 21046 USA (e-mail: kazuhiro.sakai@nasa.gov; antoine.r.miniussi@nasa.gov).

Color versions of one or more of the figures in this paper are available online at http://ieeexplore.ieee.org.

Digital Object Identifier 10.1109/TASC.2017.2655718

require a pixel count that would be impractical. However, an alternative option is to combine two different pixel designs onto the same substrate. We define this geometry as a "hybrid" array. The two types of TESs can have different sizes and designs, and hence performance capabilities in addition to the absorber being different in size. One region is optimized for looking at bright point sources with a small pixel array (SPA) and the other will be optimized for the fainter extended sources with a large pixel array (LPA). In this paper, we report on measurements of the transition properties of LPA and SPA fabricated on same substrate, utilizing different sizes and different normal metal geometry to allow simultaneous optimization of more than one pixel type. We then describe measurements of a prototype hybrid array, optimized to have different transition properties in different regions.

II. Adjusting TES Transitions by Varying Size and Geometry of Normal Metal Features

Our TESs consist of molybdenum (superconducting) and gold (normal) thin-film metal bilayers. We define the intrinsic superconducting transition temperature, T_{c_i}, as the bilayer transition temperature that is observable in the absence of any effects from superconducting leads or any added normal metal features. It is only dependent on the thickness of the Mo and the Au via the vertical proximity effect. We have previously found that the longitudinal proximity effect between the Nb superconducting leads and the TES bilayer can alter the observed superconducting transition temperature (T_c), the size of the increase from T_{c_i} becoming more substantial as the TES size decreases [5]. The origin of these shifts is due to the leads increasing the order parameter of the TES bilayer above what it would typically be, particularly in the vicinity of the leads. We have also found that TESs with a significant bias current passing through them seems to partially suppress the apparent shift in transition temperature caused by the leads [2]. We therefore need to define the temperature of the TES in the transition under its operational conditions as an X-ray microcalorimeter, as T_0. A second important physical effect to consider is the lateral inverse proximity effect, in which the transition temperature and shape can be adjusted by adding normal metal features, which will tend to reduce T_c [6]. In this section we present some data as examples of how these effects can be combined to engineer T_0, and the shape of the TES transition when operating as an X-ray microcalorimeter.

To understand the effect of device geometry for TES performance, we investigated the variation in transition properties while first varying the size of TES. We fabricated devices with square bilayer dimensions of 100, 120 and 140 μm, all with the same bilayer properties and thus the same T_{c_i} on a test chip with an 8 $\times$ 8 array of pixels with mixed TES size, but all with the same size absorber. The R vs T curves for the three different sized TESs with a bath temperature of 55 mK is shown in Fig. 1. These curves are derived from current-voltage measurements, and knowledge of the thermal conductance of each pixel type determined by measuring IVs at a large number of temperatures [7]. These devices have 2.37 μm thick gold absorbers with 'T'-shaped contact (stem) regions between the substrate and the absorbers that are cantilevered up above the substrate in the non-stem regions [8]. The TESs also have gold "stripes" on top of the bilayer that extend across the TES perpendicular to the current flow, and gold "banks", deposited along the edge of the TESs parallel to the direction of bias current flow. The stripes are known to broaden the transitions slightly and reduce so-called "excess-noise" in TESs in the 100-140 μm size range, leading to better energy resolution X-ray microcalorimeters [9]. The gold banks ensure that the TES properties are not affected by excess current along the side edges associated with small fabrication variations in the bilayer edges. The transition temperatures and shapes are quite similar, but are changing in a systematic way with TES size. As can be seen in Fig. 1, as the TES size decreases, the lower regions of the transitions move toward lower temperature, and the transition widths become broader. In addition, their normal resistances are quite different, as the effect of the normal metal features in reducing the TES resistance has a proportionally larger effect as the TES size decreases. We observe that for these devices the net effect of the combination of the proximitization from the leads and the stripes produces a shift lower with decreasing TES size and decreasing distance between normal metal stripes and stem ('S'). We also note that by adjusting the TES size, we not only affect the transition properties, but also the thermal conductance to the heat bath which scales with the perimeter of the TES [10].

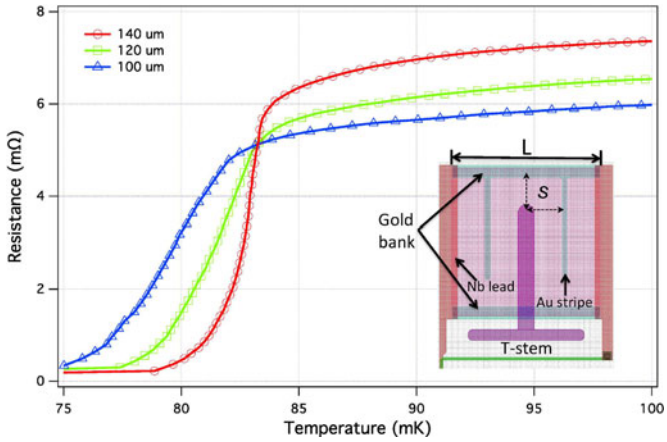

Fig. 1. Measured resistance versus temperature curves for three different sized TESs (L=100, 120 and 140 μm) which have same intrinsic transition temperature, T_{c_i}. There are gold stripes and an absorber support 'stem' perpendicular to the direction of the bias current flow, and "banks" parallel to it. These structure contribute to both mechanical stability of bilayer and detector performance.

A second example that shows very clearly how the TES transition temperature and shape changes with the addition of different metal structures, is shown in Fig. 2. In this figure, the transition curve for the TES with a Au stripe pattern added, shifts the transition temperature by more than 30 mK for a bilayer with a T_{c_i} of 135 mK. And the slope of the transition with stripes becomes broader. The only difference between the two geometries is that the added three gold stripes branch out from the gold banks that run on the edge of the TES. The added Au stripes, which are deposited on top of the bilayer, depresses the order parameter in the lateral vicinity around the structure [6]. Therefore, we can

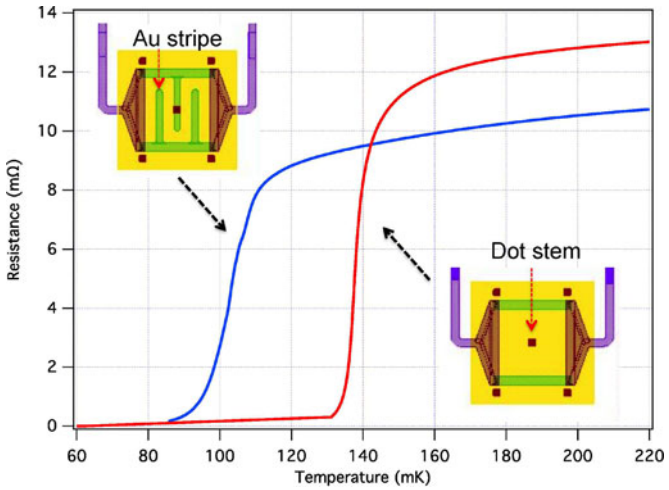

Fig. 2. Measured resistance versus temperature curves with different normal metal geometry on the 67 μm small size Mo/Au bilayer. The stripes change the transition temperature and its shape. The small stems (black regions) are needed to support for absorber and the center stem provides thermal contact between the TES and cantilevered absorber above it, without shorting it out.

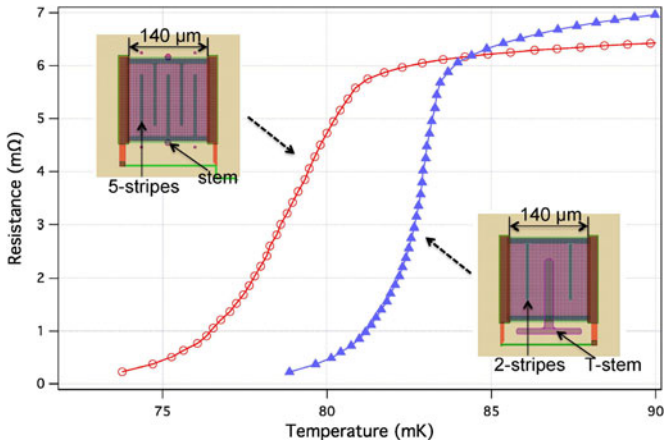

Fig. 3. Resistance versus temperature curves for two 140 μm sized TESs. One of the TESs has two Au stripes and an extended Au stem region, and the other has five Au stripes and two small stem regions.

use the addition of normal metal stripes in addition to adjusting the TES size, to tune the TES properties.

A third example here shows how the addition of Au stripes only is used to affect the transition temperature and shape in large TES geometries of a fixed size. However, the shifts in T_c are less dramatic than in smaller TESs. Fig. 3 shows plot of the transition curves of two 140 μm TESs with nominally the same bilayer properties, fabricated at the same time and within 2 mm of each other. One TES has a geometry very similar to those in Fig. 1, with gold banks, two Au stripes, and a stem region in contact with the absorber that extends across the center of the TES. The other has 5-stripes in addition to a stem region contacting the absorber. The 5-stripe pattern clearly has a significantly lower T_c, about 5 mK lower than the 2-stripe one.

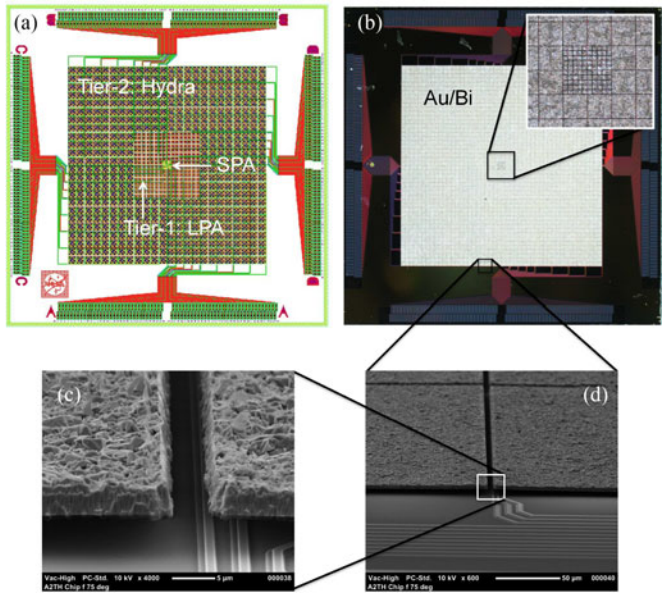

Fig. 4. (a) Schematic diagram of a prototype hybrid pixel array design. (b) Photograph of fully fabricated hybrid array with Au/Bi absorbers. (c) and (d) are scanning electron micrograph images of the absorbers.

The shape of the transition curve is extremely important to consider, because it will affect both the energy range over which the X-ray microcalorimeter has high performance, and the energy resolution that can be achieved. The full width at half maximum energy resolution of TES is expressed as [11]

$$\Delta E_{\mathrm{FWHM}} = 2\sqrt{2ln2}\sqrt{\frac{4k_b {T_0}^2 C}{\alpha}\sqrt{1+2\beta}} \qquad (1)$$

where C and T_0 denote the device heat capacity and operating temperature, $\alpha = \frac{T_0}{R_0}\frac{\partial R}{\partial T}$ and $\beta = \frac{I_0}{R_0}\frac{\partial R}{\partial I}$ describe the dependence of the resistance on temperature and current, and R_0 and I_0 are the resistance of and the current passing through the TES.

Since α and β will vary as the TES size varies, and also as normal metal features are added, as well as T_c, it is important to optimize the energy resolution and dynamic range for the different pixel types. To achieve this, it will be necessary for the fabrication process to be extremely precise. The large-pixel TESs with 2-stripe patterns, with TES size in the range of 100-140 μm, typically have α's in the range of $\sim$50-100 and β's in the range of $\sim$1-2 in the region of the transition that provides the best energy resolution (typically 15-20% of the TES normal resistance). Ref. [4] provides all the desired pixel parameters for potential different pixel types in the Athena X-IFU, where the properties of both SPA and LPA pixels are adjusted to be optimized independently.

III. Prototype Hybrid Array

We have developed a prototype array that demonstrates how useful it can be to adjust the transition properties in different regions, which allows them to be optimized differently. A layout diagram and photograph of this hybrid array is shown in Fig. 4. In the center, is a 10 $\times$ 10 array of small pixels on a 50 μm

pitch. Surrounding the central array in the first "tier" is a 16 × 16 of larger pixels on a 250 μm pitch. Then around the outside, in the second tier, the array of 250 μm pixels is extended to 48 × 48 using a 24 × 24 array of 4-absorber "hydras" [12], except in the inner regions of the center and first-tier arrays. In each hydra here, a single TES is attached to four different absorbers via thin film metal thermal links of different thermal conductances. By discriminating between the pulse-shapes before all four absorbers come into thermal equilibrium, such as through measuring the signal rise-time, it is relatively straightforward to discriminate in which absorber each X-ray is stopped [12]. In this type of arrangement, the central region is ideal for observing point sources with the highest energy resolution and with the highest count rate capability. The first tier is ideal for looking at extended sources with relatively high spatial and energy resolution. The second tier extends the field-of-view by a factor of 9 in area, maintaining the same spatial resolution as the first tier and degrading the energy resolution by about 30-50%, while only approximately doubling the number of TESs that need to be read out.

The fabrication of a hybrid array is significantly more complicated than a single uniform array [13]. In particular, up until now, small pixels have been fabricated onto solid silicon substrates into which a thin layer of copper is buried just below the surface of the wafer, with a thin layer of silicon oxide on top of it [14]. The solid substrate is necessary in small pixels to provide a relatively strong thermal conductance to the substrate, determined by the thermal boundary resistance [15], and the buried copper layer is necessary to maintain a uniform heat-sink temperature for all the pixels and minimize thermal cross-talk [14]. However single pixels and hydras on the size-scale of 250 μm use TESs deposited on silicon nitride membranes to produce the required thermal conductance to the heat-sink, with a support grid of silicon beams coated in back-side copper being used to provide the thermal and mechanical support. The buried copper layer needed for the small pixels and the membrane layer needed for the larger pixels therefore had incompatible fabrication processes. To overcome this, a new approach was used for the heat-sinking of the small pixels, in which the whole small-pixel array was fabricated on a free-standing silicon nitride membrane as well, and then copper is deposited onto the back-side of this membrane to provide the heat bath and to lower thermal cross-talk [13].

What is key to the design of the hybrid array is the engineering of the TES transitions to optimize the energy resolution, dynamic range of X-ray energies, and the X-ray count-rate capabilities of each pixel type independently. This was achieved using the transition-engineering techniques described in the previous section. The array shown in Fig. 4 is the first prototype developed, and has a Mo/Au bilayer with a T_{c_i} of 70 mK using thicknesses of 50 nm and 245 nm for the Au and Mo layers respectively. Then copper 1.4 μm thick was deposited directly onto the backside of the SiN membrane underneath the innermost array, and to the backside of support grid of silicon beams for the outer tiers. This layer is needed to provide sufficient heat-sinking for all pixels and to reduce the thermal cross-talk between pixels, which is especially important for the inner SPA.

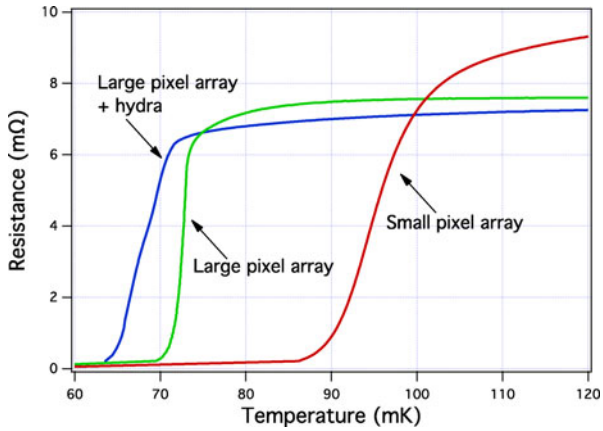

Fig. 5. Resistance versus temperature curves for each of the three pixel types in the prototype hybrid array.

This inner array consists of small pixels which require a relatively high T_c. We therefore used a small TES that is 25 μm in size, with no added metal features on the TES, to keep the T_c as high as possible. In the first prototype, this T_c was approximately 120 mK at low currents. The full transition curve under bias with a heat-sink temperature of 55 mK is shown in Fig. 5.

A small pixel with this T_c is capable of providing ∼1 eV energy resolution [15]. Indeed, an achievable energy resolution of around 0.6 eV (the achievable energy resolution was determined from integrating the noise-equivalent power) was observed. For the first tier of pixels, the energy resolution needs to be optimized as much as possible, and so there is a TES that is 140 μm in size, and has three normal metal stripes on the TES. In the first prototype, the stripes slightly reduced the T_c to 68 mK, and optimized the transition shape and noise to provide an achievable energy resolution of around 2 eV for the energy range of 0.2-7 keV [16].

Then in the second tier, the hydras utilized a TES that was also 140 μm in size, but which had 5 normal metal stripes on them to keep the T_c as low as possible. Since the hydras each have 4 absorbers they have relatively high heat capacity. Therefore they have very large dynamic range, and can remain linear in their signal responses up to 7 keV for much lower temperatures than the single pixels. By lowering the T_c, we can reduce the heat capacity and the intrinsic thermodynamic noise [17]. In our first prototype, this T_c was measured to be 63 mK. Thus the achievable energy resolution should be able to scale a little better than the $\sim\sqrt{n}$ (where n is the number of absorbers in the hydra) [12]. In our first prototype some irregular additional "kink" features in the transitions were observable, and can be seen in Fig. 5. These are understood as being due to stress in the first prototype designs, that meant that this scaling could not be verified. Future versions of the hydra design will have modifications to try to reduce such effects.

In this example the absorber composition of all three pixel types are the same. The absorbers consisted of a bilayer of gold (1.5 μm) and bismuth (3.0 μm). The thin gold provides rapid lateral thermalization across each 250 μm absorber, while the bismuth adds high quantum efficiency for stopping X-rays up to

7 keV. A more optimal design would have the same absorbers for the first tier and second tier arrays, but would utilize all-gold absorbers in the small pixels for greater dynamic range, and for even more rapid pixel thermalization. Some new innovative fabrication techniques have recently been developed that will allow this suggested more optimal varied composition of absorbers in the different regions of the array, allowing the heat capacity to be optimized for a range of sizes and energy ranges [13].

Another feasible approach to adjusting T_c of TESs in different regions of arrays, is to adjust the gold thickness so that one region has a different thickness to the other. We have recently begun to test the practicality of this approach and some first tests have been made. We found that the T_{c_i} could be increased by around 20 mK by removing 30 nm thick of a gold layer in a Mo/Au film, without affecting the overall width and properties of the TES transition. We estimate that even higher changes of $\sim$40 mK should be achievable by removing 50 nm thick of gold from a sub-region of the bilayer. This approach will also be incorporated into future hybrid arrays.

IV. Conclusion

Because the transition temperature and shape of TESs is so highly dependent upon the function the size of the TES and the normal metal features on top of it, we can design hybrid arrays consisting of pixels with very different required transitions on a single substrate, utilizing a bilayer with just one intrinsic T_{c_i}. Here we have demonstrated this transition engineering capability for the first time. Further optimization by fabricating different absorbers in attached to the different TESs will help make further hybrid arrays a very useful option for future X-ray astronomy missions.

References

[1] M. E. Eckart *et al.*, "Kilopixel X-ray microcalorimeter arrays for astrophysics: Device performance and uniformity," *J. Low Temp. Phys.* vol. 167, pp. 732–740, Jan. 2012.

[2] S. J. Smith *et al.*, "Small pitch transition-edge sensors with broadband high spectral resolution for solar physics," *J. Low Temp. Phys.* vol. 167, pp. 168–175, Feb. 2012.

[3] D. Barret *et al.*, "The Athena X-ray Integral Field Unit (X-IFU)," in *Proc. SPIE*, vol. 9905, Aug. 2016, Art. no. 99052F.

[4] S. J. Smith *et al.*, "Transition-edge sensor pixel parameter design of the microcalorimeter array for the X-ray Integral Field Unit on Athena," in *Proc. SPIE*, vol. 9905, Jul. 2016, Art. no. 99052H.

[5] J. E. Sadleir, S. J. Smith, S. R. Bandler, J. A. Chervenak, and J. R. Clem, "Longitudinal proximity effects in superconducting transition-edge sensors," *Phys. Rev. Lett.*, vol. 104, no. 4, Jan. 2010, Art. no. 047003.

[6] J. E. Sadleir *et al.*, "Proximity effects and nonequilibrium superconductivity in transition-edge sensors," *Phys. Rev. B*, vol. 84, no. 18, Nov. 2011, Art. no. 184502.

[7] P. L. Richards, "Bolometers for infrared and millimeter waves," *J. Appl. Phys.*, vol. 76, no. 1, Mar. 1994, pp. 1–24.

[8] C. A. Kilbourne *et al.*, "Uniform high spectral resolution demonstrated in arrays of TES X-ray microcalorimeters," in *Proc. SPIE*, vol. 6686, Sep. 2007, Art. no. 668606.

[9] J. N. Ullom *et al.*, "Characterization and reduction of unexplained noise in superconducting transition-edge sensors," *Appl. Phys. Lett.*, vol. 84, May 2004, Art. no. 4206.

[10] H. F. C. Hoevers, M. L. Ridder, A. Germeau, M. P. Bruijn, P. A. J. De Korte, and R. J. Wiegerink, "Radiative ballistic phonon transport in silicon-nitride membranes at low temperatures,"*Appl. Phys. Lett.*, vol. 86, no. 25, Jun. 2005, Art. no. 251903.

[11] K. D. Irwin and G. C. Hilton, "Cryogenic particle detection," in *Topics in Applied Physics*, C. Enss, Ed. Berlin, Germany: Springer-Verlag, 2005.

[12] S. J. Smith *et al.*, "Development of position-sensitive transition-edge sensor X-ray detectors," *IEEE Trans. Appl. Supercond.*, vol. 19, no. 3, pp. 451–455, Jun. 2009.

[13] E. Wassell *et al.*, "Fabrication of X-ray microcalorimeter focal planes composed of two distinct pixel types," *IEEE Trans. Appl. Supercond.*, vol. 27, no. 4, Jun. 2017, Art. no. 2300205.

[14] F. M. Finkbeiner *et al.*, "Development of embedded heatsinking layers for compact arrays of X-ray TES microcalorimeters," *IEEE Trans. Appl. Supercond.*, vol. 21, no. 3, pp. 223–226, Jun. 2011.

[15] S. R. Bandler *et al.*, "Advances in small pixel TES-based X-ray microcalorimeter arrays for solar physics and astrophysics," *IEEE Trans. Appl. Supercond.*, vol. 23, no. 3, Jun. 2013, Art. no. 2100705.

[16] S. J. Smith *et al.*, "Uniformity of kilo-pixel arrays of transition-edge sensors for X-ray astronomy," *IEEE Trans. Appl. Supercond.*, vol. 25, no. 3, Jun. 2015, Art. no. 2100505.

[17] D. McCammon, "Cryogenic particle detection," in *Topics in Applied Physics*, C. Enss, Ed. Berlin, Germany: Springer-Verlag, 2005.